A kinetic study for NO catalytic reduction on silica sub-micron diameter tubes with platinum nanoparticles

Juana M. Rosas, Ramiro Ruiz-Rosas, José Rodríguez-Mirasol*, Tomás Cordero

Universidad de Málaga, Andalucía Tech, Dpto. de Ingeniería Química, 29071 Málaga, Spain

ABSTRACT

The selective catalytic reduction (SCR) of NOx with C_3H_6 in the presence of O_2 on silica sub-microtubes with platinum nanoparticles was studied in order to establish a possible reaction mechanism at different experimental conditions. This catalyst showed a high NO conversion with very high selectivity to N_2 at mild conditions in the presence of excess oxygen when using C_3H_6 as reducing agent.

The influence of both NO and C_3H_6 concentrations on their conversions was analyzed at different space times. The obtained results suggest that the three reactants (C_3H_6, NO, and O_2) are adsorbed on Pt sites. The kinetic model proposed considers that both dissociative adsorption of NO and activation of the hydrocarbon can take place simultaneously. Nevertheless, the value of the parameters obtained by the resolution of the model equations indicates that the first one presents a major relevance. These results are in concordance with the high selectivity to N_2 observed, because the preponderance presence of dissociated NO avoids the formation of N_2O by the reaction of molecular NO with N dissociated from NO. Furthermore, both NO reduction and C_3H_6 oxidation conversions are represented reasonably well by the model presented.

Keywords: NOx; SCR; platinum; nanoparticles; silica nanotubes; coaxial electrospinning; reaction mechanism

1. INTRODUCTION

NO_x (NO & NO_2) exhausted from vehicles and stationary combustion engines is one of the important causes of photochemical smog, acid rain, and ozone depletion, which possess serious challenges to human health and environmental protection [1]. Selective catalytic reduction (SCR) technology with hydrocarbons is believed to be one of the most promising options for DeNOx [2]. However, SCR usually requires rather high reaction temperature (over 300 ◦C) when hydrocarbons (HCs) or CO are used as reducing agents [3]. If SCR of NOx with HC occurs at low temperature over catalyst with high DeNOx activity, the technology could compete with NH_3-SCR and be more practical for the removal of NOx at stationary or mobile sources [1].

Catalysts based on platinum have been pointed out as potential candidates for this process. Obuchi et al. (1993) demonstrated that at lower temperatures (typically below 300 ◦C) these metals could catalyze NOx reduction by the hydrocarbons found in the exhaust (e.g. propane and propylene) under lean-burn conditions [4]. It is found that Pt has the highest NOx reduction activity under lean conditions among the platinum group metals [5,6]. However, this high activity is accompanied by low N_2 selectivity, i.e. large quantities of N_2O are formed over Pt under lean conditions [5]. And N_2O is an important greenhouse gas and air pollutant, having much more impact per unit mass (global warming potential) than carbon dioxide according to the Environmental Protection Agency (EPA) [7].

Regarding the reaction mechanism, the technical literature proposes two main reaction pathways for low temperature selective catalytic reduction of NO on Pt catalysts. The first one involves production of molecular nitrogen through NO dissociative adsorption via a redox mechanism [8,9]. According to this scheme, NO is adsorbed on the Pt

surface and dissociates to yield adsorbed nitrogen and oxygen atoms, which desorb in the form of molecular N_2 and/or N_2O, due to the reaction between two dissociated nitrogens and by one dissociated nitrogen and molecular NO, respectively. The role of the reductant is to react with adsorbed oxygen atoms and regenerate the active sites. The other mechanism proposes that the activation of the hydrocarbon plays the key role in the lean-DeNO_x reaction. In this sense, the activated hydrocarbon can react with adsorbed NO or NO_2 [10-12] to form organo-nitro species that later decomposes as N_2 or N_2O. It has been also suggested that the adsorbed hydrocarbon can react with NO to form $C_xH_yO_zN_w$ species [13,14], which would be later removed from the surface by reaction with oxygen, thus regenerating the active sites.

This research group has reported results on the preparation and characterization of silica sub-microtubes loaded with platinum nanoparticles, which showed a high activity and total selectivity to N_2 at mild conditions, in the presence of excess oxygen, when using C_3H_6 as reducing agent [15]. Therefore, the aim of this work is to deepen into the behavior of this catalyst on this process, analyzing its performance under different experimental conditions to establish a possible mechanism for NO reduction by C_3H_6 in the presence of O_2. The experimental results have been correlated with a kinetic model that represents adequately these experimental data.

2. MATERIALS AND METHODS

2.1. Catalyst preparation

The silica sol was prepared from tetraethyl orthosilicate (TEOS), ethanol, distilled water, and HCl. The sol composition in molar ratio was 1:2:2:0.025 (TEOS:ethanol:water:HCl). Platinum (II) acetylacetonate was added to the solution in a

molar ratio to TEOS of 0.006. A more detailed explanation of the sol gel preparation can be found elsewhere [15].

Silica sub-microtubes were generated by using the coaxial electrospinning method reported in the literature [16] in a co-axial configuration, with the sol gel, which plays the role of carrier, coming through the external capillary tip and synthetic oil flowing through the inner one. The flow rates through the needles were around 0.6/1.5 $mL \cdot h^{-1}$ for sol gel/synthetic oil, respectively. To apply the high voltage between the spinneret and the collector, two high voltage power supplies are used: one positively polarized connected to the needle and the other one negatively polarized attached to a collector. The tip-to-collector distance was 20–25 cm, and the electrical potential difference was 10 kV (the collector was at –5 kV and the tips at +5 kV).

The electrospun tubes with platinum, denoted as SiT-Pt, were easily collected as a flexible non-woven mat, and were calcined at 500ºC for 2 hours in order to stabilize them.

2.2. Catalyst characterization

A deep characterization was already performed and reported [15]. In this work, the surface chemistry of the samples before and after the reaction at different experimental conditions was studied by X-ray photoelectron spectroscopy (XPS) analysis, using a 5700C model Physical Electronics apparatus with MgKα radiation (1253.6 eV). For the analysis of the XPS peaks, the C1s peak position was set at 284.5 eV and used as reference to locate the other peaks. The fitting of the XPS peaks was done by least squares using Gaussian-Lorentzian peak shapes.

The surface and inner morphology of the tubes was studied by scanning electron microscopy (SEM) using a JSM 840 JEOL microscope working at 25 KV voltage and

by transmission electron microscopy (TEM) in a Philips CM200 microscope at an accelerating voltage of 200 kV and in a high angle annular dark field (HAADF)FEI Titan G2.

2.3 NO Selective Catalytic Reduction (SCR) experiments

The NO reduction experiments were performed in a quartz fixed bed microreactor (4 mm i.d.) at atmospheric pressure. Experiments were carried out with 80 mg of catalyst. The total flow rate was varied from 100 to 250 cm^3 STP/min for different concentrations of NO ranging from 200 to 800 ppm and C_3H_6 from 200 to 1500 ppm. The concentrations of other inlet gases were 3% for O_2 and 200 ppm for N_2O. A chemiluminiscent analyzer (EcoPhysics, CLD 700 AL model) was used to measure the outlet gas concentrations of NO and NO_2. The CO and CO_2 outlet concentrations were analyzed by means of a non-dispersive infra-red analyser (Ultramat 22, Siemens model). C_3H_6, H_2O, N_2, N_2O and O_2 concentrations were measured by a mass spectrometer analyzer (Balzers MsCube).

2.4. Kinetic analyses

The mathematical equations to describe the NO reduction rates in the presence of propylene (as reducing agent) and oxygen are obtained by establishing the kinetic rate equation and then solving the molar balance to the fixed-bed reactor. The following assumptions were taken into account: homogeneous distribution of active sites on the catalyst surface; axial dispersion was discarded by adequate fixed bed length and reactor geometry (L/D>20); the reactor operated at steady-state conditions; diffusional constraints and transport limitations were negligible; and changes in temperature and pressure within the reactor were neglected.

Plug flow integral reactor can be used for the interpretation of the experimental data. To this purpose the reactor mass balance equations (1) and (2) were numerically and simultaneously integrated to calculate the exit conversion of the NO reduction and C_3H_6 oxidation reactions,

$$\frac{dX_{NO}}{d\left(\frac{W}{F_{NO}}\right)} = r_{NO} \qquad \therefore \int_0^{X_{NO}} dX_{NO} = \int_0^{W/F_{NO}} r_{NO}\, d\left(\frac{W}{F_{NO}}\right) \tag{1}$$

$$\frac{dX_{C3H6}}{d\left(\frac{W}{F_{C3H6}}\right)} = r_{C3H6} \qquad \therefore \int_0^{X_{C3H6}} dX_{C3H6} = \int_0^{W/F_{C3H6}} r_{C3H6}\, d\left(\frac{W}{F_{C3H6}}\right) \tag{2}$$

where r_{NO} and r_{C3H6} represent the reaction rates of nitric oxide reduction and propylene oxidation ($mol \cdot s^{-1} \cdot g^{-1}$), respectively; X_{NO} and X_{C3H6} are the total conversions of NO and propylene, and (W/F_{NO}) and (W/F_{C3H6}) are the nitric oxide and propylene space times, respectively. The reaction progress towards each product formation can be calculated in the same way if required.

The dependence with the temperature of the kinetic and thermodynamic parameters, involved in the proposed mechanisms, was considered to follow the Ahrrenius (3) or the Van't Hoff law (4), respectively,

$$k_i = k_{oi} \exp\left(\frac{-E_{ai}}{RT}\right) \tag{3}$$

$$K_i = K_{oi} \exp\left(\frac{-\Delta H_i}{RT}\right) \tag{4}$$

where k_{oi} and K_{oi} are the pre-exponential factors, E_{ai} the activation energy of the reaction (i) and ΔH_i the enthalpy of the equilibrium (i). The optimization of the Arrhenius and

Van't Hoff parameters involved in these equations were performed by minimizing the objective function:

$$O.F. = \sum_i \left(X_i^{\exp} - X_i^{cal} \right)^2 \qquad (5)$$

where X_i^{exp} represents the value of the experimental conversions of the reactives involved in the model proposed and X_i^{cal} the ones calculated by solving the differential rate equations system by a modified Runge-Kutta method with Matlab 2013b software. The minimization of the equation (5) was based on the Levenberg-Marquart algorithm. The optimized kinetic parameters are used to simulate the conversion profiles at different temperatures, initial gas pressures, NO and propylene space times and inlet compositions.

3. RESULTS AND DISCUSSION

Figures 1a and b present SEM and TEM micrographs of the catalyst, respectively. As can be seen, the catalyst used consists of submicrometric tubes, very uniform in size and shape. The submicrometric tubes present total BET surface area of 144 m^2/g and around 1% (wt) of Pt. Figure 1 c and d despite high-angle annular dark field scanning transmission electron microscopy (HAADF-STEM) image of the wall of the submicrotube. The micrographs show the presence of well-dispersed platinum nanoparticles of around 2 nm. Furthermore, the selected electron diffraction pattern of the Pt nanoparticles suggests the mainly presence of metallic platinum.

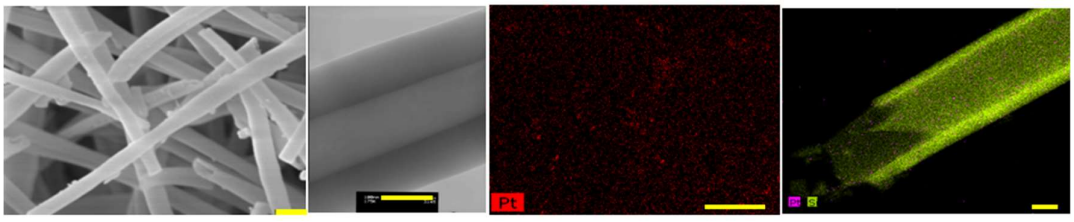

Figure 1. a) SEM image, bar length (1μm); b) TEM micrograph of the catalyst, bar length (100 nm); c) HAADF-STEM of the catalyst surface (Pt:red particles) , bar length (50 nm); d) HAADF-STEM of submicrotubes (Pt:pink particles; Si: green particles) , bar length (50 nm).

Figure 2 shows the evolution of outlet gas concentration as a function of the reaction time for an experiment where the inlet gases were added sequentially to the catalyst previously described. Initially, only NO diluted in He (200 ppm, W/F_{NO} = 2.88 g·s/μmol) was introduced in the reactor at 210 ºC. After around 60 min, O_2 (3% vol) was added to the inlet stream and, finally, at around 120 min of reaction time, C_3H_6 (1500 ppm) was also introduced. In the first step only a low adsorption of NO was observed and no reaction products were detected. With the addition of oxygen to the inlet stream, about 50% of NO is oxidized to NO_2, due to the well-known high activity of metallic platinum as oxidation catalyst. With the addition of C_3H_6, the presence of NO_2 in the outlet gases is practically negligible. In this sense, some authors suggested that propylene is strongly adsorbed on the catalyst surface, decreasing the surface coverage of oxygen. This fact reduces the probability of the NO and O adsorption at adjacent vacant sites, and so, the presence of propylene may be considered to inhibit the surface oxidation of NO to NO_2 [3,17-19]. In this step, the conversion of NO is slightly improved; however, the selectivity is total to N_2. No formation of N_2O was detected, at least, within our detection limits, suggesting that NO was quickly dissociated, and no molecular NO adsorption was taken place [17,18,20], avoiding the formation of N_2O that is one of the main drawbacks reported in the literature for platinum catalysts [11,21,22]. Regarding propylene, there is not an equimolar ratio between NO and propylene converted, because the reductant is also able to be directly oxidized by oxygen at this reaction temperature, producing equals amounts of CO_2 and H_2O.

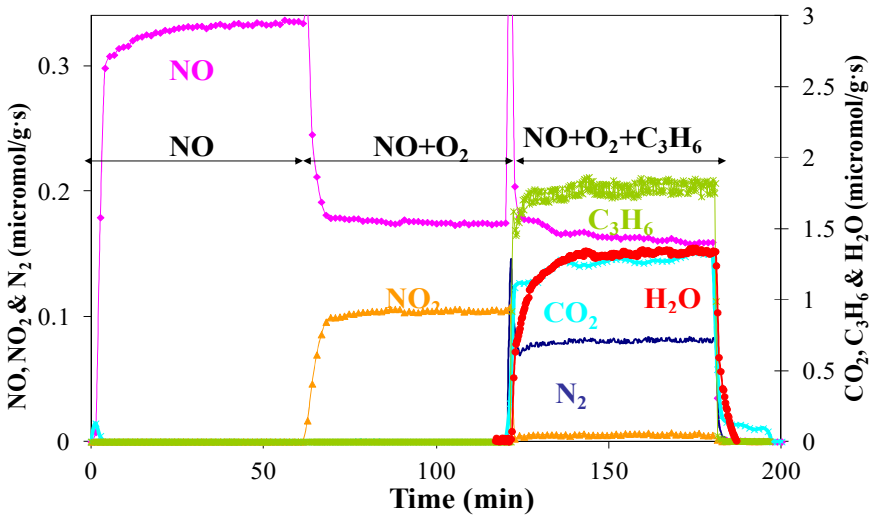

Figure 2. Evolution of outlet gas concentration as a function of reaction time, with 200 ppm_V NO, 3%v O_2 and 1500 ppm_v C_3H_6, at 210 ºC, W/F_{NO} = 2.88 g·s/µmol.

The stability of the catalyst under different experimental conditions is another important aspect for catalytic applications. The good behavior observed for the catalyst under atmospheres containing SO_2 was already reported in a previous work [15]. Now, the activity of the catalyst was evaluated at different reaction temperatures and inlet concentrations, and no signals of deactivation were observed. As an example, Figure 3 represents the NO conversion as a function of the time on stream with 200 ppmv NO, 1500 ppmv C_3H_6 and 3% O_2, at 200 ºC, W/F_{NO}= 2.88 g·s/µmol. As can be seen, the catalyst showed the same activity along the experiment, with the same selectivity toward N_2 and the corresponding characterization analyses of the catalyst after 8 hours of reaction indicated no significant changes on its properties.

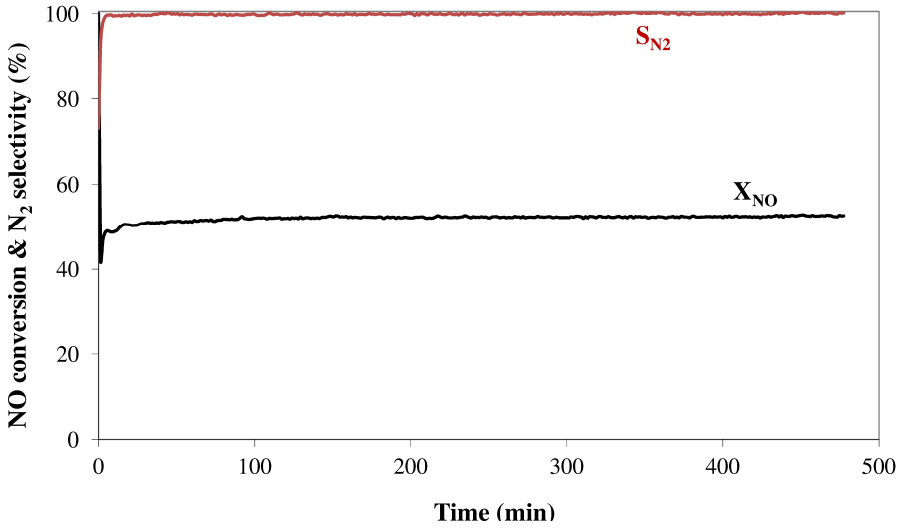

Figure 3. NO conversion and N_2 selectivity as a function of time on stream with 200ppmv NO, 1500ppmv C_3H_6 and 3% O_2, at 200 ºC, W/F_{NO}= 2.88 g·s/µmol.

3.1. Influence of NO concentration on its reduction

The effect of NO concentration on the SCR with 1500 ppmv C_3H_6 and 3% O_2 was evaluated at different temperatures and at fixed W/F_{NO}= 1.92 g·s/µmol. Figure 4.a-b shows the corresponding NO and C_3H_6 conversions as a function of NO inlet concentration at different reaction temperatures, respectively. As can be seen, the NO conversion increases, at a fixed space velocity, as the NO inlet concentration does. The increase of the propylene conversion is not as high as the one observed with NO, at the same experimental conditions, due to the competitive adsorption between both reactants, being NO adsorption favored with respect to the propylene one. For conversions lower than 20%, a differential mode of operation can be assumed in this plug flow reactor. Furthermore, as the inlet conversion is zero, the following equation can be used to determine an apparent reaction order with respect to NO conversion:

$$F_{NOo} \cdot \frac{X_{NO}}{W} = r_{NO} = k_{ap} \cdot C_{NO}^{n} \qquad (1)$$

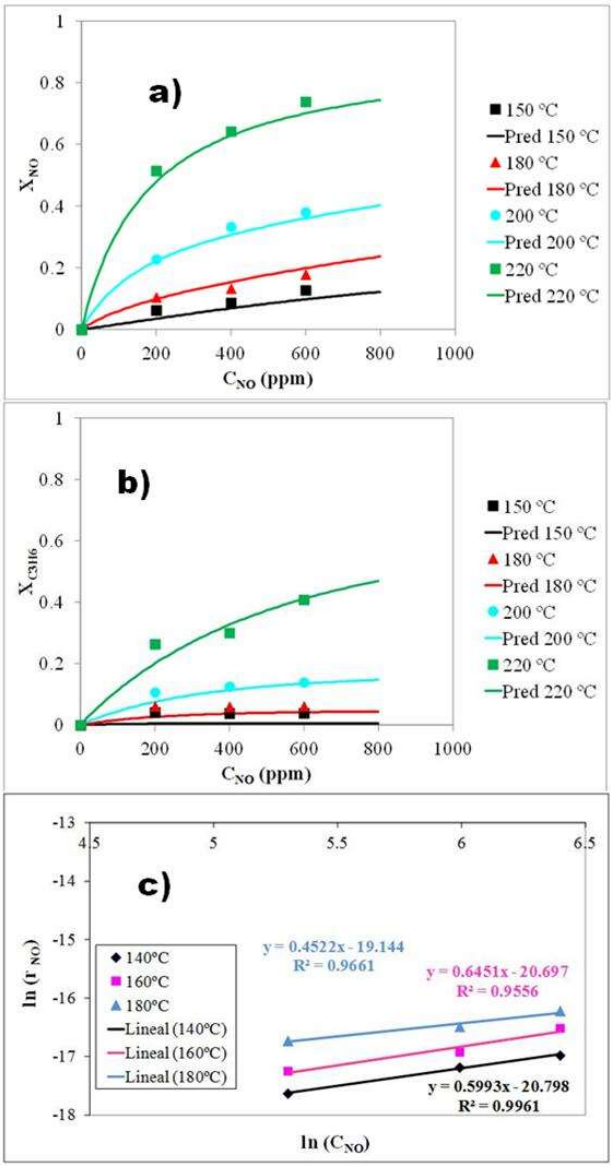

Figure 4. a-b) NO and C_3H_6 conversion as a function of NO inlet concentration, respectively, with 1500ppmv C_3H_6 and 3% O_2, at different reaction temperatures, and at fixed W/F_{NO}= 1.92 g·s/µmol (symbols: experimental data; solid lines: predicted data); c) Natural logarithm of the NO reaction rate as a function of the logarithm of the NO inlet concentration.

Figure 4.c represents the natural logarithm of the NO reaction rate as a function of the logarithm of the NO inlet concentration. The apparent reaction orders were found to be

222 approximately 0.5 with respect to NO concentration, at the different temperatures
223 evaluated. This half-order dependence suggests that the dissociative adsorption of NO
224 must be probably involved in the reaction mechanism with this catalyst, under these
225 conditions (temperatures lower than the one needed to reach the maximum NO
226 conversion), in agreement with the redox mechanism proposed by Burch et al. [5,8,9].

227 *3.2. Influence of C_3H_6 concentration on NO reduction*

228 The influence of C_3H_6 concentration on NO reduction was analyzed by varying C_3H_6
229 concentration from 200 to 1500 ppmv, with 200 ppmv NO and 3% O_2, at different
230 reaction temperatures and at fixed W/F_{NO}= 2.88 g·s/μmol. NO conversions as a function
231 of the reaction temperature at different C_3H_6 concentrations are shown in Figure 5.a.
232 The results clearly indicated that NO reaction is favored at higher propylene
233 concentrations. Denton et al. (2001) reported that NO reduction strongly depends upon
234 the θ_{HC}/θ_O ratio. For NO to be reduced, θ_{HC} must be high enough to protect the surface
235 from oxidation by O_2 and to permit NO adsorption [23]. Besides, the presence of
236 propylene may be considered to inhibit the surface oxidation of NO to NO_2
237 [3,17,18,19]. In this sense, NO conversion with 200 ppmv C_3H_6 at 220 ºC was 28.6%,
238 being the selectivity to NO_2 approximately 12%. However, the NO conversion with 800
239 ppmv C_3H_6, at the same reaction temperature, was 64.2%, obtaining in this case, a
240 selectivity value to NO_2 lower than 2%. The rest was converted to N_2. With 1500 ppmv
241 C_3H_6, the selectivity to NO_2 was negligible. In contrast, all NO converted was
242 selectively reduced to N_2. All these results suggest that NO to C_3H_6 molar ratios higher
243 than one must be used to obtain a high and selective NO reduction to N_2. In agreement
244 with these results, Denton et al. (2001) observed that N_2 selectivity is also strongly
245 enhanced by the increase of C_3H_6 inlet concentration [23].

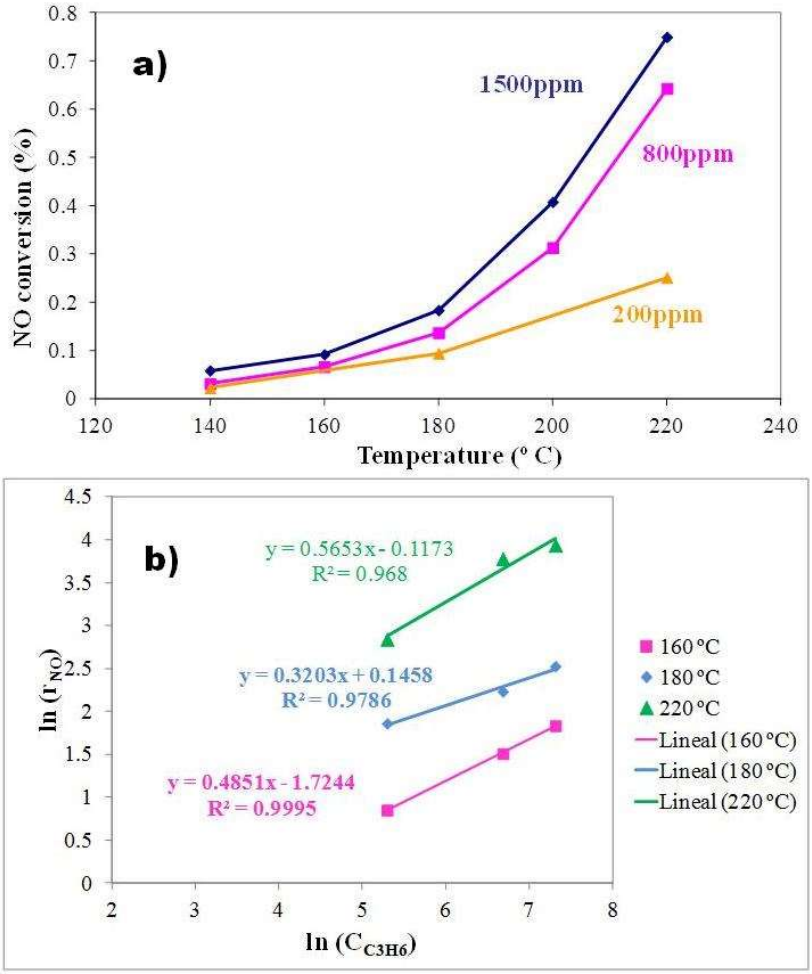

Figure 5. a) NO conversions as a function of the reaction temperature at different C_3H_6 concentrations, with 200 ppmv NO and 3% O_2, and at fixed W/F_{NO}= 2.88 g·s/µmol. b) Natural logarithm of the NO reaction rate as a function of the logarithm of the C_3H_6 inlet concentration.

To evaluate the dependence of NO reduction rate on C_3H_6 concentration, the natural logarithm of the NO reaction rate as a function of the logarithm of the C_3H_6 inlet concentration at different reaction temperatures, was represented in Figure 5.b. Half-order dependence with respect to C_3H_6 inlet concentration was also observed, which can be associated to the activation of the reductant by dissociative adsorption. These results

are also in concordance with the formation of a carbonaceous intermediate on the active Pt sites that can react with NO.

3.3. Influence of NO concentration on C_3H_6 oxidation

The range of application of this kind of catalyst strongly depends on its ability to perform the activation (oxidation) of the reductant. Therefore, it is quite important to analyze the behavior of the catalyst with respect to the reducing agent. For this goal, the oxidation of propylene was tested with this catalyst at different propylene concentrations in the presence and absence of NO. Figure 6.a collects the propylene conversions as a function of the reaction temperature with different inlet concentrations, but in these experiments W/F_{C3H6} was not constant. As can be seen, this catalyst is very active for the propylene oxidation at the temperature range studied, obtaining a total conversion of propylene at 200 ºC, with 200 ppmv C_3H_6, and 60% with 1500 ppmv C_3H_6. The addition of only 200 ppmv NO shifted the oxidation curve to higher temperatures; in this case, the temperature must be increased about 40 ºC to observe the same propylene conversion. Some authors pointed out that C_3H_6, NO, and O_2 are adsorbed on the same type of Pt adsorption sites [21]. So, it seems that this inhibition may be directly related to active site occupation by atomic N produced by NO dissociation and/or adsorbed nondissociated NO molecules. In this case, NO surface coverage on the Pt surface must be higher than the one corresponding to O_2, thus decreasing the probability of propylene combustion [3,22].

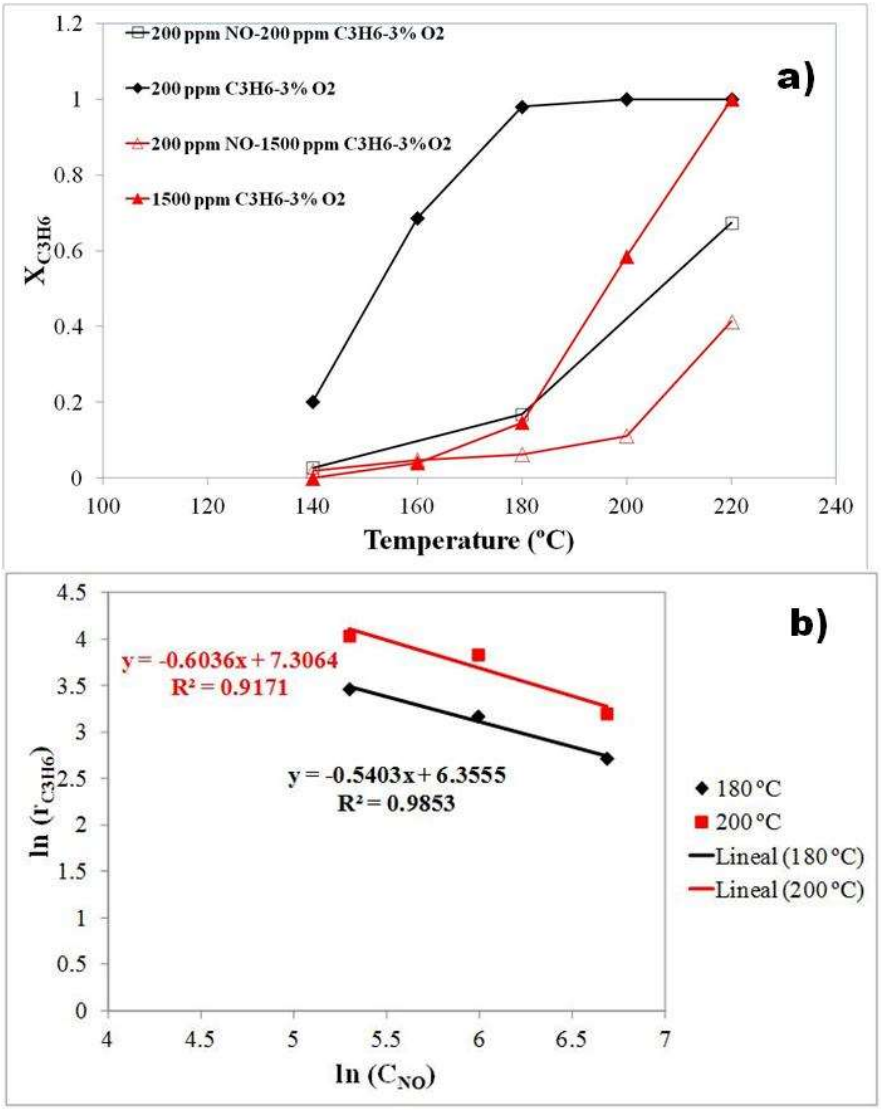

277

278 Figure 6. a) Propylene conversions as a function of reaction temperature at different
279 inlet concentrations, with 200 ppmv NO and 3% O_2, and at fixed W/F_{NO}= 2.88
280 g·s/µmol. b) Natural logarithm of the C_3H_6 reaction rate as a function of the logarithm
281 of the NO inlet concentration, at fixed W/F_{C3H6}= 0.38 g·s/µmol.

282

283 To study how the NO concentration affects to the rate expression of propylene
284 oxidation, C_3H_6 inlet concentration was fixed to 1500 ppmv and NO concentration was
285 varied from 200 to 800 ppmv, with 3% O_2, at different reaction temperatures(W/F_{C3H6}=
286 0.38 g·s/µmol). Figure 6.b. shows the natural logarithm of the C_3H_6 reaction rate as a

function of the logarithm of the NO inlet concentration, at different reaction temperatures. As can be observed, a negative half-order term with respect to NO was obtained at these experimental conditions. These results also support the partial inhibition of the propylene oxidation due to the possible presence of strongly (and apparently dissociatively) adsorbed NO, in agreement with the results reported by Nikolopoulos et al. [23].

3.4. Influence of N_2O concentration on NO reduction

One of the main drawbacks reported in the literature for platinum catalysts is the formation of N_2O. Its formation during NOx SCR is mainly associated to the reaction between adsorbed N (derived from the dissociative adsorption of NO) and NO molecularly adsorbed [11,17,21,22]. However, some authors proposed that N_2O is an intermediate for N_2 formation [22].

A negligible outlet gas concentration of N_2O was observed with this catalyst at the experimental conditions studied, in agreement with the results observed by Yang and Jung using H_2 as reducing agent. These authors found that only N_2O was formed at low temperatures, meanwhile the formation of N_2 was predominant at temperatures over 80 °C [24].

This finding can be associated to two different hypotheses: a) the dissociative adsorption of NO is so fast, that the presence of NO molecularly adsorbed is negligible; b) if N_2O is an intermediate for N_2 formation, the transformation reaction of N_2O to N_2 must be very quick. To analyze the role of N_2O, two different kinds of experiments were carried out. Firstly, the reaction of N_2O was evaluated at several conditions: with only 200 ppmv N_2O, with 200 ppmv N_2O and 3% O_2 and with 200 ppmv N_2O, 1500 ppmv C_3H_6 and 3% O_2; all of them at 200 ºC and a space velocity of 2.88 g·s/µmol. The

311 conversion of N_2O was negligible at these conditions. In this sense, Konsolakis et al.
312 (2012) observed that N_2O reacted at temperatures higher than 300 ºC [25].

313 On the other hand, an experiment with 200 ppmv NO, 200 ppmv N_2O, 1500 ppmv C_3H_6
314 and 3% O_2 was also performed. Figure 7 shows a comparison between the NO
315 conversion as a function of the reaction temperature in the presence and absence of
316 N_2O. The profile was very similar in both cases, which seems to indicate that the
317 formation of N_2 does not take place via N_2O intermediate.

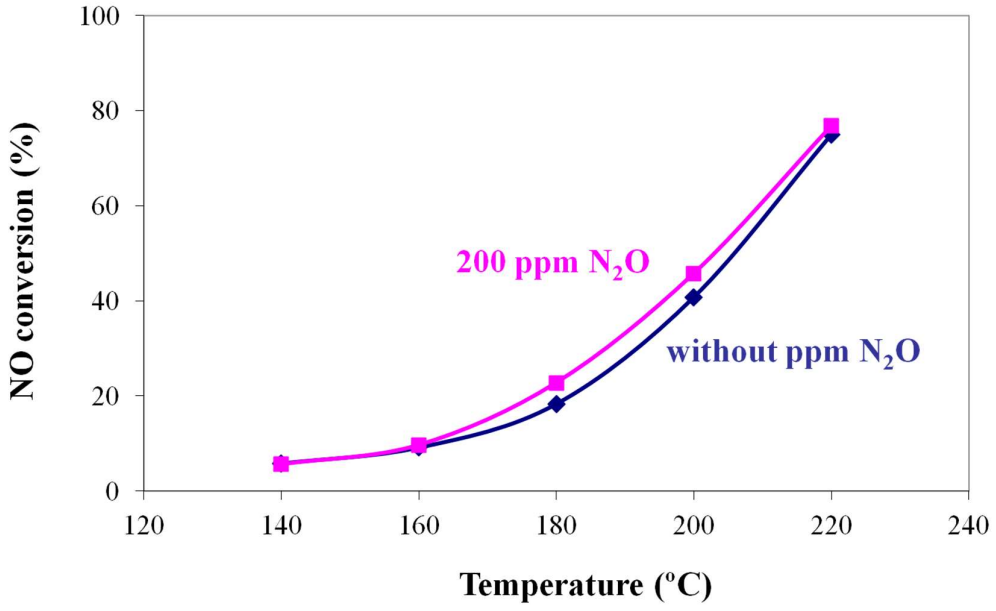

318

319 Figure 7. NO conversion as a function of the reaction temperature in the presence and
320 absence of 200 ppmv N_2O, with 200 ppmv NO, 1500 ppmv C_3H_6 and 3% O_2.

321

322 *3.5. Role of O_2 on NO reduction*

323 Figure 8 shows the evolution of outlet gas concentration as a function of the reaction
324 time for an experiment where the inlet gases were added sequentially. Initially, only 3%
325 O_2 was introduced in the reactor at 210 ºC. After around 60 min, NO diluted in He (200
326 ppm, W/F_{NO} = 2.88 g·s/µmol) was added to the inlet stream and, finally, at around 120

min of reaction time, C_3H_6 (1500 ppm) was also introduced. Some differences can be noticed by comparing the second step of this figure with the one shown in Figure 2, corresponding to the oxidation of NO. The NO conversion is the same in both cases (48%), but a prompt evolution of NO_2 can be observed in Figure 2. On the contrary, a certain induction time in the formation of NO_2 appears in Figure 8 and the time required to achieve a pseudo steady state in this last experiment is much longer than the one represented in Figure 2, where the steady state is immediately reached.

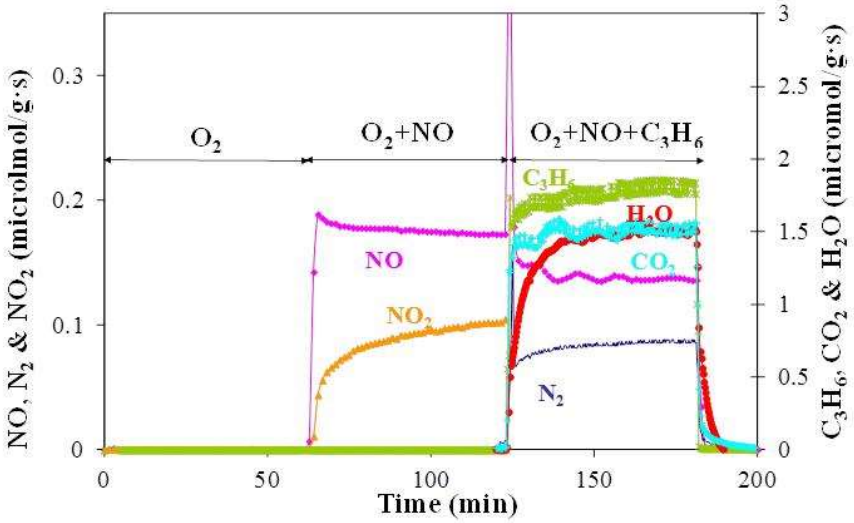

Figure 8. Evolution of outlet gas concentration as a function of reaction time, with 3%v O_2, 200 ppm_V NO and 1500 ppm_v C_3H_6, at 210 ºC, W/F_{NO} = 2.88 g·s/µmol.

With the sequence NO-NO+O_2, the NO surface coverage must be quite high and the addition of oxygen produces the rapid reaction to NO_2. In contrast, the previous addition of O_2 seems to imply O_2 adsorption and when NO is added to the inlet stream, this must be then adsorbed, probably, displacing oxygen from the Pt active sites. The long time required to achieve a pseudo steady state in this case seems to indicate that a large NO surface coverage is required for its oxidation to take place and that the surface

344 population of O_2 must be significantly decreased. On the other hand, it is important to
345 mention that once the steady state is reached, only 65% of the NO converted evolved as
346 NO_2 at the outlet stream, suggesting either the partial adsorption of NO or the formed
347 NO_2. In this sense, Khosravi et al. (2014) analyzed different kinetic models reported in
348 the literature for the oxidation of NO, preferentially based on Eley-Rideal models, and
349 even including the possible inhibition effect of the NO_2 adsorbed [26]. Similarly,
350 Denton et al. also observed that NO_2 reacts with propylene to only NO nor N_2 or N_2O
351 [22]. Therefore, these results could indicate that the large initial evolution of NO (see
352 Figure 8) when propylene was added is related to the reaction between adsorbed NO_2
353 and propylene. Then, when steady state is reached, the preferential formation of N_2 is
354 detected.

355 In order to clarify if there is a competition between NO and O_2 with our catalyst for the
356 active sites with a preferential adsorption of NO or if O_2 is completely displaced by NO
357 at this temperature, different experiments were performed. Firstly, the catalyst was
358 treated with a stream containing only NO (200 ppmv) at 200 ºC, then a temperature
359 programmed desorption (TPD) was carried out up to 500 ºC. All NO adsorbed was
360 desorbed at the same temperature (physisorption), without any evolution during TPD.
361 The same experiment was carried out but using 3% O_2, at the same temperature, and, in
362 the same way, the oxygen adsorbed was evolved during the desorption step, with a
363 negligible evolution during the TPD. The adsorption of O_2 was also analyzed at 260 ºC;
364 the adsorbed amounts were quite similar at 200 and 260 ºC, and in neither of both
365 experiments the evolution of O_2 was detected during TPD.

366 The same experiment was carried out but only using 3% O_2, at 200 ºC and 260 ºC. The
367 oxygen adsorbed was similar in both experiments and all of it evolved during the
368 desorption step, with a negligible evolution during the TPD.

In another test, the NO adsorption was also evaluated at 200 ºC, but in this case, the catalyst used was previously reacted with NO-O_2-C_3H_6 at 260 ºC. The corresponding results are shown in Figure 9. As can be seen, an important and exponential O_2 evolution was observed during the treatment with NO, which takes place simultaneously to a decrease of the NO concentration. Furthermore, a low formation of NO_2 can be also noticed. The adsorption of oxygen seems to be very stable at the highest temperature range. During the desorption step, all NO adsorbed was completely desorbed. These results suggest that O_2 is greatly adsorbed on Pt surface in the absence of other gases in the inlet stream or at high temperatures (temperatures higher than the one at which the maximum NO conversion is obtained, Tmax). The addition of NO at low temperatures produces the displacement of oxygen from the Pt active sites.

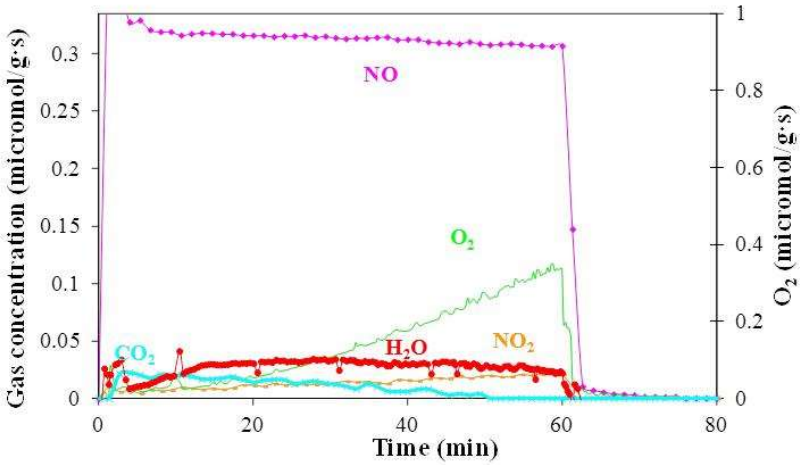

Figure 9. Evolution of outlet gas concentration as a function of reaction time, with 200 ppmV NO, at 210 ºC, after reacting with NO-O_2-C_3H_6 at 260 ºC.

Finally, the catalyst was treated with 3% O_2 at 260 ºC for 1 h and then the oxygen was desorbed at the same temperature. At this temperature, a stream containing 1500 ppmv C_3H_6 was fed for 1 h, and subsequently desorbed. Then, the catalyst was cooled to 200 ºC and followed by a TPD up to 500 ºC. The adsorption of O_2 was close to 6 mmol/g.

388 During the desorption step at 260 ºC, the amount of O_2 desorbed (corresponding to
389 physisorbed O_2) was 5.66 mmol/g. So, 0.34 mmol/g of O_2 must remain strongly
390 adsorbed on the catalyst surface. With the addition of propylene at 200 ºC, a low
391 formation of CO_2 can be observed (0.035 mmol/g). The evolution of oxygen was not
392 observed, in this case. Therefore, it seems that the oxidation of propylene is favored,
393 instead of the displacement of oxygen from the active sites, at this high temperature.
394 During the cooling step, an additional CO_2 evolution was also detected (0.28 mmol/g),
395 suggesting that all O_2 adsorbed was available for the reductant oxidation. In agreement
396 with these results, Garcia Cortes et al. (2007) reported that the surface coverage of
397 oxygen is very low and there exists a direct competition between NO and O_2 for Pt
398 adsorption sites, being favorable to NO, at temperatures below Tmax. However, the
399 catalyst surface is mainly covered by oxygen species at temperatures higher than Tmax
400 [19]. In this line, Li et al. also found a competitive adsorption between NO and O_2 with
401 a Pt/SAPO-34 catalyst, but using CO as reducing agent [27].

402 *3.6. Reaction mechanism*

403 *3.6.1. NO oxidation*

404 This reaction is exothermic and is limited by its equilibrium at high temperatures. There
405 are many works in the literature which deals with the oxidation of NO on platinum
406 catalyst. An Eley–Rideal-type mechanism involving dissociative adsorption of O_2 and
407 reaction of NO from gas phase is mostly used to model the NO oxidation reaction on Pt
408 catalysts [28-30]. However, the results obtained in the present work by adding the gases
409 sequentially seem to indicate that a certain NO surface coverage is required for the
410 oxidation reaction to take place. In this sense, some authors have found that a

411 Langmuir-Hinshelwood model is more adequate to model the NO oxidation reaction
412 [31,32]. Therefore, the following reactions are proposed to describe the NO oxidation:

413 $$* + NO \overset{K_{NO}}{\longleftrightarrow} * NO \quad (2)$$

414 $$* + O_2 \overset{K_{O2}}{\longleftrightarrow} * O_2 \quad (3)$$

415 $$* + \ * O_2 \overset{K_{O2d}}{\longleftrightarrow} 2 * O \quad (4)$$

416 $$* NO + * O \overset{k_{NO2}}{\longrightarrow} * NO_2 + * \quad (5)$$

417 $$* NO_2 \overset{K_{NO2}}{\longleftrightarrow} NO_2 + * \quad (6)$$

418 Reaction 2 makes reference to the equilibrium adsorption of NO. O_2 adsorption is
419 assumed to proceed through a molecular precursor (reaction 3), followed by the
420 dissociation of the precursor to atomic oxygen (reaction 4), due to oxygen dissociation
421 on Pt surface proceeds via a precursor-mediated reaction path [31]. Reaction 5 considers
422 the surface reaction between NO adsorbed and dissociative oxygen adsorbed to form
423 NO_2. The equilibrium adsorption of the NO_2 formed is represented in Reaction 6. This
424 last reaction is supported by the work of Mulla et al. (2006). They included a certain
425 inhibition effect in the kinetic model due to the adsorbed NO_2, which partially inhibited
426 the Pt active sites [32].

427 Some authors reported that adsorbed NO predominantly covers the catalyst surface at
428 low temperatures (<150 ºC), which is due to its high sticking coefficient on Pt. As the
429 temperature is increased, the surface becomes predominantly covered with O until, at a
430 very high temperature (~400 ºC), adsorbed O starts desorbing as O_2, which results in an
431 increase in the vacant site coverage [31].

3.6.2. NO reduction with C_3H_6

As aforementioned, two main reaction mechanisms are reported in the literature to describe the NO reduction in the presence of propylene and oxygen. The first one involves production of molecular nitrogen through NO dissociative adsorption via a redox mechanism. The other mechanism proposes, in a simplified way, that the activated hydrocarbon react with NO or NO_2 to finally decomposes to N_2 or N_2O.

Based on the results previously commented, the following reactions can be also considered in the mechanism for the low temperature SCR:

$$* + * NO \overset{K_{NOd}}{\longleftrightarrow} * N + * O \quad (7)$$

$$* + C_3H_6 \overset{K_{C3H6}}{\longleftrightarrow} * C_3H_6 \quad (8)$$

$$* C_3H_6 + * O \xrightarrow{k_{C3H6}} * C_3H_6O + * \quad (9)$$

$$* C_3H_6O + 4O_2 \xrightarrow{k'_{C3H6}} 3CO_2 + 3H_2O + * \quad (10)$$

$$* N + * N \xrightarrow{k_{N2}} N_2 + 2 * \quad (11)$$

$$* C_3H_6O + * NO \xrightarrow{k''_{C3H6}} * C_3H_6NO_2 + * \quad (12)$$

$$* C_3H_6NO_2 + * NO + 3O_2 \xrightarrow{k'''_{C3H6}} N_2 + 3CO_2 + 3H_2O + 2 * \quad (13)$$

The three reactants (C_3H_6, NO, and O_2) are suggested to be adsorbed on the same type of Pt adsorption sites (denoted as $*$). However, in this case, the kinetic constants of reactions (3) and (4), corresponding to O_2 adsorption, must be significantly decreased at temperatures lower than Tmax, due to the surface coverage of oxygen is rather low at these temperatures. Reactions (5) and (6) are not going to be taken into account in the

kinetic model, due to the fact that the formation of NO_2 in the presence of propylene is lower than 5% at best, and besides, its reduction produces the formation of NO nor N_2 or N_2O [22].

A half-order dependence with respect to NO was observed for the NO reduction rate, what suggests that the dissociative adsorption of NO must be probably involved in the reaction mechanism, under the experimental conditions tested (temperatures lower than the one needed to reach the maximum NO conversion). This mechanism is represented by reactions (7) and (11). Nevertheless, the possibility of a mechanism based on the activation of the hydrocarbon cannot be completely ruled out. Therefore, it has also been considered in reactions (12) and (13), as pointed by Zheng et al. [33].

On the other hand, the absence of N_2O at the outlet stream can indicate the low presence of NO molecularly adsorbed on the catalyst surface. Furthermore, it is also observed that the formation of N_2 does not take place via N_2O intermediate. So, the formation of N_2O has not been considered in this reaction mechanism.

With regard to the role of oxygen, Captain et al. (2000) also reported that molecular oxygen could be involved in the reaction pathway [11] and Nikolopoulos et al. (1990) found a first-order dependence of NO reduction and C_3H_6 oxidation on O_2 for Pt/alumina, suggesting the possibility of direct participation of O_2 from the gas phase in the activation of the reductant or the removal of carbonaceous deposits [23]. In our case, the reduction of NO with propylene in the absence of oxygen was negligible, and only with the addition of oxygen was observed a significant NO conversion [15]. Besides, the results above described suggest that the surface coverage of oxygen at temperatures lower than Tmax is very low, so, the participation of oxygen from the gas phase in the

475 NO reduction has been considered in this reaction mechanism by reactions (10) and
476 (13).

477 Finally, reaction (9) and (10) make reference to the own oxidation of propylene in the
478 presence of oxygen. Although this oxidation is partially inhibited in the presence of NO,
479 the amount of propylene oxidized is higher than the amount of NO reduced. Therefore,
480 they must be included in the mechanism. Some authors even suggested that in the lower
481 temperature region the activation of the hydrocarbon appears to be the kinetically
482 significant step. Such a claim is supported by the observed delay in the hydrocarbon
483 light-off in the presence of NO, the close proximity of the ascending part of the NO
484 reduction curves and the corresponding hydrocarbon oxidation curves, and the coupling
485 between the points of maximum NO conversion and complete hydrocarbon oxidation
486 [8].

487 On the other hand, it is important to clarify that reaction (13) is not a direct reaction, but
488 it involves the formation of different intermediates. However, no physical evidences of
489 the possible intermediates are observed in these experiments, and the literature is not
490 clear about this aspect. For this reason and for the sake of simplicity, this reaction has
491 been considered by one unique step. However, a possible reaction pathway could be as
492 follows:

493 $$* C_3H_6NO_2 + * NO \rightarrow C_2H_6 + N_2 + CO_2 + * O \quad (14)$$

494 $$C_2H_6 + * O \rightarrow C_2H_4 + H_2O + * \quad (15)$$

495 $$C_2H_4 + O_2 \rightarrow CH_4 + CO_2 \quad (16)$$

496 $$CH_4 + * O \rightarrow * CH_2 + H_2O \quad (17)$$

$$* CH_2 + * O \rightarrow * CH_2O + *$$ (18)

$$* CH_2O + O_2 \rightarrow H_2O + CO_2 + *$$ (19)

3.6.3. Rate equations and kinetic study

By considering, the adsorption equilibriums of NO, O_2 and C_3H_6 over the platinum site (reactions 3-5,8), and assuming that the surface coverage of dissociated oxygen and nitrogen are the same, it can be obtained:

$$\theta_{NO} = K_{NO} \cdot C_{NO} \cdot \theta_f$$ (20)

$$\theta_{O_2} = K_{O2} \cdot C_{O2} \cdot {\theta_f}^2$$ (21)

$$\theta_{C_3H_6} = K_{C_3H_6} \cdot C_{C_3H_6} \cdot \theta_f$$ (22)

$$\theta_N = \theta_O = (K_{NOd} \cdot \theta_{NO} \cdot \theta_f)^{0.5}$$ (23)

Taking into account quasi steady-state for the formation rate of $*C_3H_6O$ intermediate, and by considering reaction (13) much faster than reaction (12), the presence of $*C_3H_6NO_2$ intermediate can be ruled out. So, the following expression can be drawn:

$$\theta_{C_3H_6O} = \frac{k_{C_3H_6} \cdot \theta_{C_3H_6} \cdot \theta_O}{k'_{C_3H_6} \cdot C_{O2}^4 + k''_{C_3H_6} \cdot \theta_{NO}}$$ (24)

Therefore, the site balance for the platinum active sites can be written as follows:

$$1 = \theta_f + \theta_{NO} + \theta_{O_2} + \theta_{C_3H_6} + \theta_N + \theta_O + \theta_{OC_3H_6}$$ (25)

Finally, it is also considered that the NO reaction rate can be expressed as a combination of the contribution of the NO reduction by the redox mechanism, and by the activation of the hydrocarbon with the following reaction with NO adsorbed. Meanwhile, the

516 oxidation of propylene can be considered to take place directly by its reaction with
517 oxygen and also by its interaction with NO:

518 $$r_{NO} = -k_{N2} \cdot {\theta_N}^2 - 2 \cdot k''_{C3H6} \cdot \theta_{C_3H_6O} \cdot \theta_{NO} \quad (26)$$

519 $$r_{N_2} = -\frac{1}{2} \cdot r_{NO} \quad (27)$$

520 $$r_{C_3H_6} = -k'_{C3H6} \cdot \theta_{C_3H_6O} \cdot {C_{O2}}^4 - k''_{C3H6} \cdot \theta_{C_3H_6O} \cdot \theta_{NO} \quad (28)$$

521

522 The values obtained for the kinetics parameters and the kinetic constant values at 180
523 ◦C, for the NO reduction in the presence of propylene are shown in Table 1. The
524 parameters obtained by the resolution of the model equations indicate that the redox
525 mechanism, proposed by Burch et al. (5,8-9) presents a major relevance than the
526 mechanism of activation of the hydrocarbon, showing kinetic constant values at 180 ºC
527 at least three orders of magnitude higher for the redox mechanism than those obtained
528 for the activation of the hydrocarbon. These results are in concordance with the high
529 selectivity to N_2, because the majority presence of dissociated NO avoids the formation
530 of N_2O by the reaction of molecular NO with N dissociated from NO.

531 Figure 4.a also represents as solid lines the estimated NO conversion as a function of
532 NO inlet concentration at different reaction temperatures and at a fixed space velocity of
533 W/F_{NO}= 1.92 g·s/μmol. Figure 10 shows the NO and C_3H_6 conversions, respectively, as
534 a function of the space-time at different reaction temperatures (NO inlet concentration =
535 400 ppm). The solid lines represent the NO and C_3H_6 conversions obtained from this
536 mechanism. The increase of the space time leads to higher conversion values. As can be
537 seen, both NO reduction and oxidation conversions are represented reasonably well by
538 the model proposed.

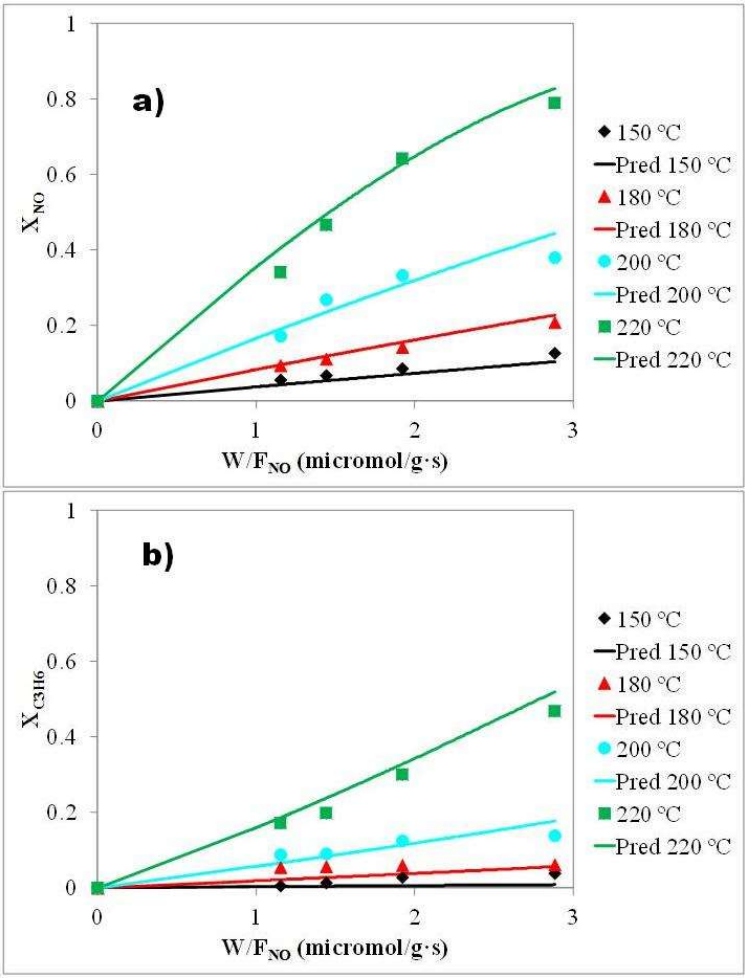

539

540 Figure 10. a) NO conversions as a function of the space time at different reaction
541 temperatures, with 1500ppmv C_3H_6 and 3% O_2, and at fixed NO concentration, 400
542 ppmv (symbols: experimental data; solid lines: predicted data); b) C_3H_6 conversions as
543 a function of the space time at different reaction temperatures, with 3% O_2, and at fixed
544 NO concentration, 400 ppmv (symbols: experimental data; solid lines: predicted data).

545

546 Table 1. Kinetic and thermodynamic parameters estimated with the proposed model.
547

	Kinetic constant value at 180 ºC		
K_{NO}	$1.63 \cdot 10^4$	K_{oNO} (M^{-1})	$1.26 \cdot 10^2$
		ΔH_{NO} (J/mol)	$-6.11 \cdot 10^3$
K_{C3H6}	$2.88 \cdot 10^3$	K_{oC3H6} (M^{-1})	$6.80 \cdot 10^3$
		ΔH_{C3H6} (J/mol)	$-3.34 \cdot 10^3$
K_{O2}	1.24	K_{oO2} (M^{-1})	$9.50 \cdot 10^{-8}$
		ΔH_{O2} (J/mol)	$-2.28 \cdot 10^4$
K_{NOd}	10.37	K_{oNOd} (-)	$1.41 \cdot 10^{-3}$
		ΔH_{NOd} (J/mol)	$-2.31 \cdot 10^3$

k_{C3H6}	$9.35 \cdot 10^{-4}$	k_{oC3H6} (-)	$2.14 \cdot 10^{7}$
		Ea_{C3H6} (J/mol)	$9.81 \cdot 10^{4}$
$k_{C3H6'}$	$1.02 \cdot 10^{-5}$	$k_{oC3H6'}$ ($mol \cdot g^{-1} \cdot s^{-1} \cdot M^{-4}$)	$6.77 \cdot 10^{0}$
		$Ea_{C3H6'}$ (J/mol)	$4.61 \cdot 10^{4}$
k_{N2}	0.062	k_{oN2} ($mol \cdot g^{-1} \cdot s^{-1}$)	$3.38 \cdot 10^{-2}$
		Ea_{N2} (J/mol)	$4.26 \cdot 10^{4}$
$k_{C3H6''}$	$1.64 \cdot 10^{-6}$	$k_{oC3H6''}$ ($mol \cdot g^{-1} \cdot s^{-1}$)	$1.74 \cdot 10^{3}$
		$Ea_{C3H6''}$ (J/mol)	$4.95 \cdot 10^{4}$

CONCLUSIONS

The kinetic study for the NO reduction, in the presence of propylene as reductant agent, and in excess of oxygen, shows half-order dependence with respect to NO inlet concentration. These results suggest that the dissociative adsorption of NO must be probably involved in the reaction mechanism, under these experimental conditions (temperatures lower than the one needed to reach the maximum NO conversion).

On the other hand, the propylene oxidation reaction shows a negative half-order term with respect to NO, at these experimental conditions. These results also support the partial inhibition of the propylene oxidation due to the possible presence of strongly (and apparently dissociatively) adsorbed NO.

The influence of NO to propylene molar ratios has been also analyzed. High and selectively NO reduction to N_2 was observed, at NO to C_3H_6 molar ratios higher than one. Furthermore, the role of N_2O on the NO reduction has been also evaluated. The results indicate that the formation of N_2 does not take place via N_2O intermediate. With regard to the role of oxygen, it seems that the addition of NO at low temperatures produces the displacement of oxygen from the Pt active sites.

Based on all the experimental results, the proposed reaction mechanism considers that the three reactants (C_3H_6, NO, and O_2) are adsorbed on the same type of Pt adsorption

sites and their corresponding fractional coverages will strongly depend on the experimental condition used. Besides, it takes into account that both the dissociative adsorption of NO and activation of the hydrocarbon can take place simultaneously. Furthermore, the participation of oxygen from the gas phase in the NO reduction has been also taken into account in this reaction mechanism. Lastly, the direct oxidation of propylene in the presence of oxygen and by its reaction with NO has also been considered.

The parameters obtained by the resolution of the model equations indicate that the redox mechanism (dissociative adsorption of NO) presents a major relevance than the mechanism of hydrocarbon activation followed by its reaction with NO. These results are in concordance with the high selectivity to N_2, because the majority presence of dissociated NO avoids the formation of N_2O by the reaction of molecular NO with N dissociated from NO. Both NO reduction and C_3H_6 oxidation conversions are represented reasonably well by the model proposed.

NOMENCLATURE

D reactor diameter [m]

E_{ai} activation energy of reaction i [kJ·mol^{-1}]

ΔHi enthalpy of reaction i [kJ·mol^{-1}]

k_i kinetic constant of reaction i [mol g^{-1} s^{-1}]

k_{oi} preexponential factor of reaction i [mol g^{-1} s^{-1}]

K_i equilibrium constants of reaction i [M^{-1}]

K_{oi} preexponential factor of reaction i [M^{-1}]

589 L bed length [m]

590 R universal gas constant [$J \cdot mol^{-1}\ K^{-1}$]

591 r_i reaction rate of reaction i [$mol \cdot g^{-1}\ s^{-1}$]

592 X_i conversion of reactive i

593 W/F_{NO} nitric oxide space time [$g\ s \cdot mol^{-1}$]

594 Greek letters

595 θ* fraction of free platinum sites

596 θ*i fractional coverage of i specie on platinum sites

597 **ACKNOWLEDGEMENTS**

598 This work was supported by the Spanish Ministry of Economy and Competitiveness
599 under CTQ2012-36408 and CTQ2015-68654-R projects.

600 **REFERENCES**

601 [1] Z. Zhang, M. Chen, Z. Jiang, W. Shangguan, J.Hazard. Mater. 193 (2011) 330.
602 [2] J. Li, J. Hao, L. Fu, T. Zhu, Z. Liu, X. Cui, Appl.Catal. A: Gen. 265 (2004) 43.
603 [3] X. Liu, Z. Jiang, M. Chen, J. Shi, Z. Zhang, W. Shangguan, Ind. Eng. Chem. Res.
604 2011, 50, 7866.
605 [4] A. Obuchi, A. Ohl, M. Nakamura, A. Ogata, K. Mizuno, Hl. Ohuchi, Appl. Catal. B
606 Environ. 2 (1993) 71.
607 [5] R. Burch, P.J. Millington, Catal. Today 26 (1995) 185.
608 [6] H. Hamada, Catal. Today 22 (1994) 21.
609 [7] http://epa.gov/climatechange/ghgemissions/gases/n2o.htm

610 [8] R. Burch, P.J. Millington, A.P. Walker, Appl. Catal. B-Environ. 4 (1994) 65.
611 [9] R. Burch, J.A. Sullivan, J. Catal. 182 (1999) 489.
612 [10] G.P. Ansell, A.F. Diwell, S.E. Golunski, J.W. Hayes, R.R. Rajaram, T.J. Truex,
613 A.P. Walker, Appl. Catal. B-Environ. 2 (1993) 81.
614 [11] D.K. Captain, Michael D. Amiridis, Catal. Today 42 (1998) 93.
615 [12] V. Pitchon, A. Fritz, J. Catal. 186 (1999) 64.
616 [13] F. Garin, P. Girard, S. Ringler, G. Maire, N. Davias, Appl. Catal. B-Environ. 20
617 (1999) 205.
618 [14] O. Gorce, F. Baudin, C. Thomas, P. Da Costa, G. Djéga-Mariadassou, Appl. Catal.
619 B-Environ. 54 (2004) 69.
620 [15] R. Ruiz-Rosas, J.M. Rosas, I.G. Loscertales, J. Rodríguez-Mirasol, T. Cordero,
621 Appl. Catal. B: Environ. 156-157 (2014) 15.
622 [16] I.G. Loscertales, A. Barrero, I. Guerrero, R. Cortijo, M. Márquez, A.M. Gañán-
623 Calvo, Science 295 (2002) 1695.
624 [17] R. Burch, J.A. Sullivan, T.C. Watling, Catal. Today 42 (1998) 13.
625 [18] I.V. Yentekakis, V. Tellou, G. Botzolaki, I.A. Rapakousios, Appl. Catal. B
626 Environ. 56 (2005) 229.
627 [19] J.M. García Cortés, M.J. Illán Gómez, C. Salinas Martínez de Lecea, ,Appl. Catal.
628 B: Environ. 74 (2007) 313.
629 [20] A. Kotsifa, D. I. Kondarides, X.E. Verykios, Appl. Catal. B: Environ. 80 (2008)
630 260.
631 [21] S.-C. Shen, S. Kawi, J. Catal. 213 (2003) 241.
632 [22] P. Denton, A. Giroir-Fendler, Y. Schuurman, H. Praliaud, C. Mirodatos, M. Primet,
633 J. Catal 189 (2000) 410.

[23] A.A. Nikolopoulos, E.S. Stergioula, E.A. Efthimiadis, I.A. Vasalos, Catal. Today 54 (1999) 439.

[24] J. Yang, H. Jung, Chem. Eng. J. 146 (2009) 11.

[25] M. Konsolakis, C. Drosou, I.V. Yentekakis, Appl. Catal. B: Environ. 123– 124 (2012) 405.

[26] M. Khosravi, C. Sola, A. Abedi, R.E. Hayes, W.S. Epling, M. Votsmeier, Appl. Catal.B: Environ. 147 (2014) 264.

[27] J. Li, G. Luo, Y. Chu, F. Wei, Chem. Eng. J. 184 (2012) 168.

[28] M. Crocoll, S. Kureti, W. Weisweiler, J. Catal. 229 (2005) 480.

[29] B. Shen, X. Lin, Y. Zhao, Chem. Eng. J. 222 (2013) 9.

[30] C. Sampara, E. Bissett, M. Chmielewski, D. Assanis, Ind. Eng. Chem. Res. 46 (2007) 7993.

[31] D. Bhatia, R.W. McCabe, M.P. Harold, V. Balakotaiah, J. Catal.s 266 (2009) 106.

[32] S.S. Mulla, N. Chen, L. Cumaranatunge, G.E. Blau, D.Y. Zemlyanov, W.N. Delgass, W.S. Epling, F.H. Ribeiro, J. Catal. 241 (2006) 389.

[33] Y. Zheng, M. Li, D. Wang, M.P. Harold, D. Luss, Catal. Today 267 (2016) 192.

Table captions

Table 1. Kinetic and thermodynamic parameters estimated with the proposed model.

Figure captions

Figure 1. a) SEM image, bar length (1μm); b) TEM micrograph of the catalyst, bar length (100 nm); c) HAADF-STEM of the catalyst surface (Pt:red particles) , bar length (50 nm); d) HAADF-STEM of submicrotubes (Pt:pink particles; Si: green particles) , bar length (50 nm).

Figure 2. Evolution of outlet gas concentration as a function of reaction time, with 200 ppm_V NO, 3%v O_2 and 1500 ppm_v C_3H_6, at 210 ºC, W/F_{NO} = 2.88 g·s/μmol.

Figure 3. NO conversion and N_2 selectivity as a function of time on stream with 200ppmv NO, 1500ppmv C_3H_6 and 3% O_2, at 200 ºC, W/F_{NO}= 2.88 g·s/μmol.

Figure 4. a-b) NO and C_3H_6 conversion as a function of NO inlet concentration, respectively, with 1500ppmv C_3H_6 and 3% O_2, at different reaction temperatures, and at fixed W/F_{NO}= 1.92 g•s/μmol (symbols: experimental data; solid lines: predicted data); c) Natural logarithm of the NO reaction rate as a function of the logarithm of the NO inlet concentration.

Figure 5. a) NO conversions as a function of the reaction temperature at different C_3H_6 concentrations, with 200 ppmv NO and 3% O_2, and at fixed W/F_{NO}= 2.88 g·s/μmol. b) Natural logarithm of the NO reaction rate as a function of the logarithm of the C_3H_6 inlet concentration.

Figure 6. a) Propylene conversions as a function of the reaction temperature at different inlet concentrations, with 200 ppmv NO and 3% O_2, and at fixed W/F_{NO}= 2.88 g·s/μmol. b) Natural logarithm of the C_3H_6 reaction rate as a function of the logarithm of the NO inlet concentration, at fixed W/F_{C3H6}= 0.38 g•s/μmol.

Figure 7. NO conversion as a function of the reaction temperature in the presence and absence of 200 ppmv N_2O, with 200 ppmv NO, 1500 ppmv C_3H_6 and 3% O_2.

Figure 8. Evolution of outlet gas concentration as a function of reaction time, with 3%v O_2, 200 ppm_V NO and 1500 ppm_v C_3H_6, at 210 ºC, W/F_{NO} = 2.88 g·s/µmol.

Figure 9. Evolution of outlet gas concentration as a function of reaction time, with 200 ppm_V NO, at 210 ºC, after reacting with NO-O_2-C_3H_6 at 260 ºC.

Figure 10. a) NO conversions as a function of the space time at different reaction temperatures, with 1500ppmv C_3H_6 and 3% O_2, and at fixed NO concentration, 400 ppmv (symbols: experimental data; solid lines: predicted data); b) C_3H_6 conversions as a function of the space time at different reaction temperatures, with 3% O_2, and at fixed NO concentration, 400 ppmv (symbols: experimental data; solid lines: predicted data).